

Determination of Direction-Independent Optical Path-Length Distribution of Cells Using Rotational-Diversity Transmitted-Light Differential Interference Contrast (DIC) Images

Chrysanthe Preza[†], Erik B. van Munster*
Jacob A. Aten*, Donald L. Snyder[†], Frederick U. Rosenberger[†]

[†]Institute for Biomedical Computing and Department of Electrical Engineering
Washington University, St. Louis, Missouri

*Laboratory for Radiobiology, Academic Medical Center
University of Amsterdam, Amsterdam, the Netherlands

ABSTRACT

Two different phase-estimation methods that have been developed for the computation of the optical path-length (OPL) distribution of a specimen from DIC images are compared in this paper. The first method is based on the Wiener filter approach and uses only a single DIC image for the determination of the OPL distribution. The second phase-estimation method is based on the conjugate-gradient optimization method and estimates the OPL distribution using rotational-diversity DIC images; i.e. multiple DIC images obtained by rotating the specimen. For this study, 24 different DIC images of a single bovine spermatozoa head were acquired by rotating the cell by approximately 15 degrees between images. The images were registered and aligned using fiducial marks, and then processed with both methods.

Results obtained with the filtering method were found to be dependent on the orientation of the cell with respect to the shear direction. Comparison of the integrated optical path length (IOPL) computed with the the filtering method and the rotational-diversity method using two, four and eight DIC images at different rotation angles showed that the IOPL estimated with the rotational-diversity method is less dependent on the rotation angle, even when only two images separated by 90-degree cell rotation are used for the phase estimation. Our results show that the use of rotational-diversity images in the determination of the OPL distribution is very beneficial because it overcomes the directional dependence of DIC imaging.

Keywords: Computational Nomarski DIC microscopy, Phase estimation, Optical path length.

1. INTRODUCTION

Contrary to other microscopy modalities, such as fluorescence and bright-field, transmitted-light Nomarski DIC microscopy^{1,2} has been limited to qualitative and morphological applications until recently. The reason for this has been the lack of computational methods applied to DIC microscopy due to the complexity of the nonlinear DIC reconstruction problem. The intensity distribution in measured DIC images is given by a nonlinear function of approximately the gradient of a specimen's optical path-length distribution (integral of refractive index over length) along the direction of shear (perpendicular to the optical axis).³ Clearly, DIC imaging is direction sensitive and does not directly provide quantitative information about a specimen's optical path-length distribution. Furthermore, the

Further author information -

C.P.: Email: preza@wuibc.wustl.edu; WWW: <http://www.ibc.wustl.edu/~preza>; Telephone: 314-362-2135; FAX: 314-362-0234

resolution in DIC images is degraded by the blurring effects of the microscope’s objective lens, as in any microscopical modality.

The recent development of model-based computational methods for Differential Interference Contrast (DIC) Microscopy⁴⁻⁷ permit the determination of the optical path-length distribution of a specimen from DIC images recorded with a CCD camera and provide a new measurement technique for biological applications. The success of some of these methods has been limited because they were developed for specific applications and are based on simplified imaging models.^{5,7} Furthermore, all these methods, except of the method developed by Preza *et al.*,^{6,8} use a single DIC image for the reconstruction (or phase estimation), and thus, they would be expected to be sensitive to the orientation of the object with respect to the DIC shear direction because of the direction sensitivity of DIC imaging. The method by Preza *et al.* overcomes this problem by estimating a specimen’s optical path-length distribution using *rotational diversity*; i.e., multiple DIC images obtained at different rotations of the specimen.

One important application of quantitative DIC imaging is determination of cell dry mass from the optical path length distribution of cells. In the early 1950s, it was shown theoretically that the optical path length integrated over a cell area is a measure of the total solid (DNA, protein) content of that cell.^{9,10} This result can now be applied to optical path-length images estimated from DIC images, and it has been investigated by van Munster, who uses DIC microscopy for the study of bovine spermatozoa. Van Munster *et al.*^{7,11} are developing a method for the computation of the optical path-length distribution of bovine spermatozoa from DIC images in order to determine a measure for the DNA and protein content of cells by summing the estimated optical path-length values of all the image pixels that fall within a cell. Because their method computes the optical path-length from a single DIC image, the accuracy of the optical path-length distribution, and thus, their measure of DNA and protein content would be expected to be affected by the orientation of the cell with respect to the shear direction. Results presented in this paper show that direction sensitivity is ameliorated when the optical path-length distribution is estimated using the rotational-diversity phase-estimation method by Preza *et al.*

In this paper, a comparison of the methods by van Munster *et al.* and Preza *et al.* is presented with results obtained from images of bovine spermatozoa heads, acquired by imaging the specimen at different rotation angles with respect to the shear direction. For the comparison, phase images were estimated from single DIC images using both methods, and from multiple DIC images using the rotational-diversity method. The integrated optical path length (IOPL) was computed from the phase images by summing the optical path-length values over a cell area and the variability of the IOPL was used as a performance measure. The paper is organized as follows. Section 2 summarizes the two computational methods compared in this paper. Section 3 describes the data acquisition and phase estimation. Finally, Section 4 compares results obtained with the two methods.

2. BACKGROUND

2.1. Rotational-diversity phase-estimation method

Details on the iterative phase-estimation method developed by Preza *et al.* and the rotational-diversity model that the method is based on were presented in earlier publications,^{3,6} but for completeness, a brief description of the method is given here. For this paper, an implementation of the method based on the coherent illumination model was used instead of the general model for partially-coherent illumination, because it is easier and faster to compute. Furthermore, the method used in this paper is regularized using a smoothness penalty (details on the regularized method can be found in¹²).

Under coherent illumination, the intensity in the k^{th} -diversity DIC-image of a specimen characterized by a transmission function $f(\mathbf{x}) = e^{-j\phi(\mathbf{x})}$ and illuminated by a quasi-monochromatic source with a mean wavelength λ and intensity a , is given by

$$i_k(\mathbf{x}) = a \left| \sum_{\mathbf{x}_0 \in \chi} f(\mathbf{x}_0) h_k(\mathbf{x} - \mathbf{x}_0) \right|^2, \quad (1)$$

where f is the object array with samples of $e^{-j\phi(\mathbf{x})}$, h_k is the array with samples of the k^{th} rotation of the point-spread function (PSF), and \mathbf{x} and \mathbf{x}_0 are three-dimensional coordinates that take values on the set $\chi = \{0, 1, \dots, N - 1\}^3$, where N is the number of elements in each dimension of the object and image space. Without loss of generality, Equation 1 models specimen rotation as a rotation of the PSF,

$$h(x, y, z) = \frac{1}{2} \left[e^{-j\Delta\theta} p(x - \Delta x, y, z) - e^{j\Delta\theta} p(x + \Delta x, y, z) \right], \quad (2)$$

by an angle, γ_k , defined as the angle that the shear direction makes with the horizontal axis, where $2\Delta\theta$ is the bias retardation (in radians), $2\Delta x$ is the shear (where it is assumed that the shear is along the x -axis), and $p(\mathbf{x})$ is the coherent PSF of the microscope's objective lens (see Goodman,¹³ p. 111). This is equivalent to modeling rotation of the direction of shear for a fixed specimen. Thus, K rotational-diversity images, $i_k(\mathbf{x})$ for $k = 0, \dots, K - 1$, have a different shear direction defined by the rotation angle γ_k . In practice, the direction of shear is fixed and rotational-diversity DIC images are obtained by rotating a specimen. Therefore, measured images need to be rotated computationally prior to processing in order to account for this difference between the model and the measured data. Also, prior to processing, measured images are corrected for CCD camera dark current and non-uniform flat-field response (see Section 3.1).

An estimate of the object's phase function, $\phi(\mathbf{x}_o)$, is obtained by minimizing the cost function,

$$E(\phi) = \sum_{k=0}^{K-1} \sum_{\mathbf{x} \in \chi} [d_k(\mathbf{x}) - i_k(\mathbf{x})]^2 + \alpha S(\phi), \quad (3)$$

which consists of the cumulative, uniformly weighted, squared-error, between K measured rotational-diversity images, $d_k(\mathbf{x})$, and the theoretical images, $i_k(\mathbf{x})$, predicted by the model in Equation 1, and a smoothness penalty, $S(\phi)$, based on Good's roughness measure,¹⁴ where α is a constant. The effect of this penalty term is to discourage discontinuities between neighboring pixel values in the estimated phase image. For a two-dimensional phase function, the penalty can be approximated using differences between a pixel and two neighboring pixels in each dimension:

$$S(\phi) = \sum_{i=0}^{N-1} \sum_{j=0}^{N-1} ([\phi(i+1, j) - \phi(i, j)]^2 + [\phi(i, j+1) - \phi(i, j)]^2 + [\phi(i-1, j) - \phi(i, j)]^2 + [\phi(i, j-1) - \phi(i, j)]^2). \quad (4)$$

Equation 3 is minimized using the well-known conjugate gradient method (see Aoki,¹⁵ p. 118). The conjugate gradient method starts from some initial guess ϕ^0 and, at iteration m , produces a new estimate for ϕ by minimizing the cost function, E , along the direction \mathbf{h}^m :

$$\phi^{m+1} = \phi^m - \beta_m \mathbf{h}^m \quad m = 0, 1, \dots \quad (5)$$

where β_m is the step size. The computation of the direction \mathbf{h}^m and of the step size, β_m , requires evaluation of the gradient vector, $\nabla E(\phi^m)$, and the Hessian matrix of E , respectively. Because it is not computationally practical to evaluate the Hessian matrix, an estimate for β_m is evaluated numerically instead using a modified line-search method based on a polynomial approximation method (Aoki,¹⁵ p. 148). For a given \mathbf{h}^m , three points of the cost function are evaluated so that they define an interval in which the cost function has a minimum. Because the minimum of a quadratic function fitted through the three points closely approximates the minimum of the cost function, the step size that minimizes this quadratic function can be used.

In general, only relative phase (or phase difference) can be estimated due to the fact that the DIC inverse problem is non-unique, and thus, the initial guess, ϕ^0 , used in Equation 5 affects the estimated absolute phase value. For many applications, only relative phase is of interest, and thus, knowledge of the absolute value of the phase is not needed. The estimated phase is also affected by the choice of value for the constant α (the weight on the penalty function) in Equation 3. It has been shown^{6,8,12} that phase images estimated with this method from measured and synthetic images of two-dimensional phantom specimens converge to a very good approximation of the specimen (up to an unknown additive constant) in the order of a few hundred iterations, at which point the change per iteration is extremely small.

2.2. Filtering method

The filtering method developed by van Munster *et al.* has been described in detail in earlier publications,^{7,11} and thus, only a summary of the method is given here. The method was initially developed for the study of bovine spermatozoa which are transparent and less than $1\mu\text{m}$ thick, and it is based on a two-dimensional geometric optics model which can be obtained from Equation 1 by ignoring the blurring effects of the PSF; i.e., by assuming an

ideal PSF which corresponds to replacing $p(\mathbf{x})$ in Equation 2 by a two-dimensional Dirac delta function. Under this approximation, the intensity in a DIC image is simply given by

$$\begin{aligned} i(x, y) &= \frac{a}{2}[1 - \cos(\phi(x - \Delta x, y) - \phi(x + \Delta x, y) + 2\Delta\theta)] \\ &= \frac{a}{2}[1 - \cos(\Delta\phi(x, y) + 2\Delta\theta)], \end{aligned} \quad (6)$$

where $\Delta\phi(x, y)$ is defined to be the difference between $\phi(x - \Delta x, y)$ and $\phi(x + \Delta x, y)$.

The filtering method consists of two parts. First, a solution for the “differential” phase image $\Delta\phi(x, y)$ is obtained from a DIC image measured at bias equal to $\pi/2$ radians by taking the arc-cosine of the normalized intensity (the intensity is normalized by the correction procedure described in Section 3.1).

Then, an estimate for the phase is obtained using the Wiener filter approach,

$$\phi(\mathbf{x}) = \mathcal{F}^{-1}\{W(\mathbf{u})\Delta\Phi(\mathbf{u})\}, \quad (7)$$

where \mathcal{F}^{-1} denotes the two-dimensional inverse Fourier transform, $W(\mathbf{u})$ is a Wiener filter, $\Delta\Phi(\mathbf{u})$ is the two-dimensional Fourier transform of $\Delta\phi(\mathbf{x})$, $\mathbf{x} = (x, y)$, and $\mathbf{u} = (u, v)$. The Wiener filter used by van Munster *et al.*¹¹ is developed to remove the effect of the latter shear, and it is given by

$$W(\mathbf{u}) = \frac{G^*(\mathbf{u})}{|G(\mathbf{u})|^2 + [1/SN(\mathbf{u})]} \quad \text{where } SN(\mathbf{u}) = s \exp(-2\pi^2\sigma^2\mathbf{u}\mathbf{u}^T), \quad (8)$$

$G(\mathbf{u})$ is the Fourier transform of the ideal PSF for bias equal to $\pi/2$ radians, G^* denotes the complex conjugate of G , s and σ are constants, and \mathbf{u}^T denotes the transpose of \mathbf{u} . The values for the constants s and σ are determined empirically and they affect the quality of the estimated phase image. As was shown in a previous publication,¹¹ with the appropriate choice of s and σ , the method is able to remove the “shadow-cast” effect (due to the DIC shearing) in DIC images.

3. METHODS

DIC images of bovine spermatozoa heads were acquired in to order to compare the two phase-estimation methods described in the previous section. In this section, the methods used to acquire and process the images are presented.

3.1. Sample Preparation and Data Acquisition

A slide of bovine spermatozoa was prepared and imaged at the Laboratory for Radiobiology, Academic Medical Center, at the University of Amsterdam, the Netherlands. The cells are flat (approximately $0.7\mu\text{m}$ thick), and they are transparent in visible light.

A straw with approximately 10 million cells of cryopreserved bovine spermatozoa (provided by Holland Genetics, Arnhem, the Netherlands) was thawed. The cells were suspended in 10 ml of phosphate buffered saline (PBS) and centrifuged at $90\times g$ for 5 minutes. The supernatant was removed, and the pellet was resuspended in 1 ml of PBS. Subsequently, the cell tails were sonicated off with a vibrating needle (20kHz, 100J). $5\mu\text{l}$ of the suspension was applied on a round coverslip (19.2mm in diameter) and was covered with a smaller coverslip (15.5mm in diameter), which was sealed with nailpolish. The large coverslip was then fitted on top of an object slide so that it could be rotated in the horizontal plane.

The images were acquired using an Ortholux II (Leitz, Germany) DIC microscope with a Leitz DIC $25\times/0.5\text{-NA}$ dry objective lens and a 0.9-NA dry condenser lens with the condenser aperture open. The DIC bias was set to approximately $\pi/2$, i.e. 1.571 radians by rotating a polarizer (de Senarmont method¹⁶). A band-pass filter (MAD8-1, Schott Glaswerke, Germany) with peak at 550nm and width 8nm around the peak was fitted in the light path, before the condenser, for quasi-monochromatic illumination. The images were acquired with a cooled CCD camera (Lambert Instruments, the Netherlands) equipped with a Kodak KAF0400 CCD chip (9- μm well size). The effective pixel size in the recorded images is $0.36\mu\text{m}\times 0.36\mu\text{m}$.

Twenty-four rotational-diversity DIC images were acquired by turning the round coverslip approximately 15 degrees between recordings. Rotation of the sample was performed manually. Landmarks, such as large air bubbles, were used to help identify the same region of the sample after each rotation.

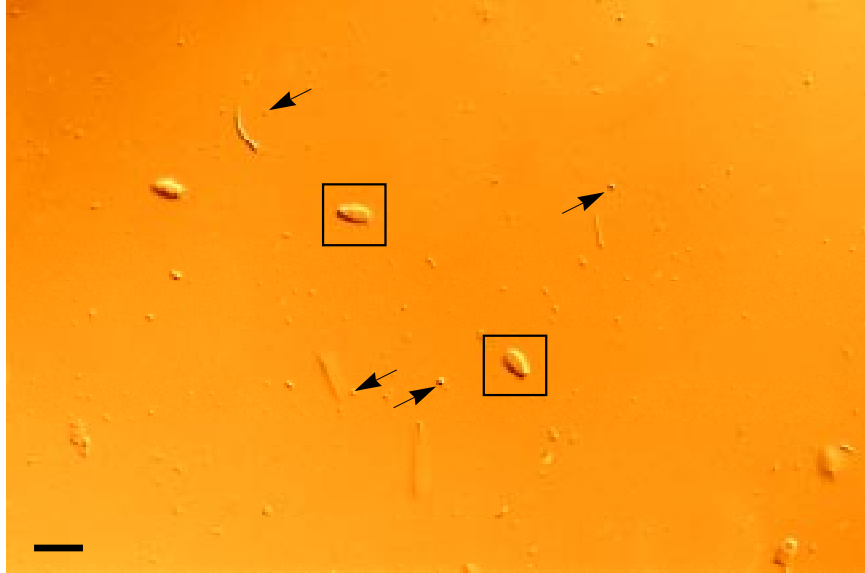


Figure 1. Measured DIC image of bovine spermatozoa heads after correction for non-uniformities due to the CCD camera response and illumination. The boxes enclose single head cells and the arrows point to small particles that were used as fiducial marks for the registration and alignment of the rotationally-diverse images. The scale bar is approximately $13.6\mu\text{m}$.

Latex spheres (460nm in diameter, DOWlatex 41984, Serva, Germany), transparent at light wavelength of 550nm, immersed in PBS were imaged at bias approximately equal to $\pi/2$ radians for the determination of the shear parameter using a procedure similar to the one described by van Munster.⁷ Calibration images, I_{min} and I_{max} , were also acquired at bias of 0 and π radians respectively of an empty region on the slide using the same exposure time as for the other images. These images were used to correct the measured DIC images for CCD camera dark current and non-uniform flat-field response, and to normalize the DIC image values. For the correction,^{11,12} I_{min} is subtracted from each DIC image and then the result is divided by $(I_{max} - I_{min})$.

3.2. Image Registration and Alignment

Because the rotation of the sample was performed manually, the angle of rotation is not accurately known. Furthermore, an inevitable translation from one rotational image to the other is introduced. Thus, in order to align the DIC images and to obtain a better estimate of the rotation angle, a simple registration procedure¹² was used. First, one of the images was selected to be the reference image. Then the angle of rotation and the translation from this reference image to all the other images was determined. This was accomplished using four fiducial marks, such as small particles (see Figure 1) identified in all the images.¹² Once the angle and translation from the reference image to the other images was estimated, a unique center of rotation was calculated for all the images thereby aligning the images. The images were then rotated accordingly (the rotation was implemented using bilinear interpolation) in order to convert cell rotation to shear direction rotation on which the rotational-diversity imaging model (Equation 1) is based. 64×64 -pixel images of a single cell were extracted from the registered images (see for example the box outlining such a region in Figure 1) for processing with the phase-estimation methods. Figures 2 and 3 show DIC images of a single cell head with fixed and rotating shear direction respectively.

3.3. Performance Measure

In order to assess the performance of the phase-estimation methods, phase images computed from single DIC images with different directions of shear are compared to phase images computed from multiple DIC images with the rotational-diversity method. For the comparison, we have used the variability of the integrated optical path-length (IOPL) value as a measure. The IOPL is computed from an estimated phase image by summing the estimated optical path-length values over all pixels that fall within the cell. A cell mask was used to identify the pixels within a cell. The cell mask was generated from an estimated phase image (obtained with the rotational-diversity method

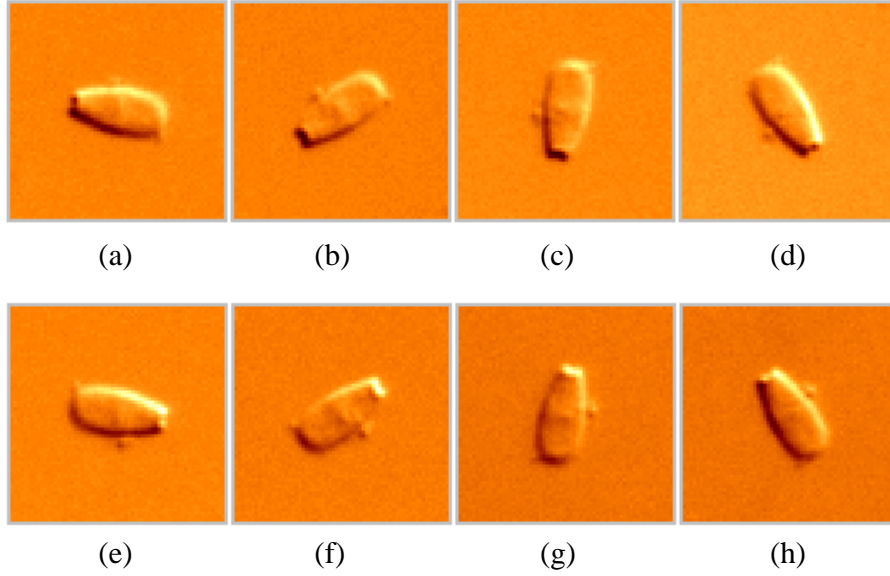


Figure 2. Measured rotational-diversity DIC images of a single bovine sperm head at different orientations of the cell. The cell was rotated every time approximately 45 degrees counter clockwise from (a) to (h). The direction of shear is along the 45-degrees axis in all the images. The field of view is $23\mu\text{m}\times 23\mu\text{m}$.

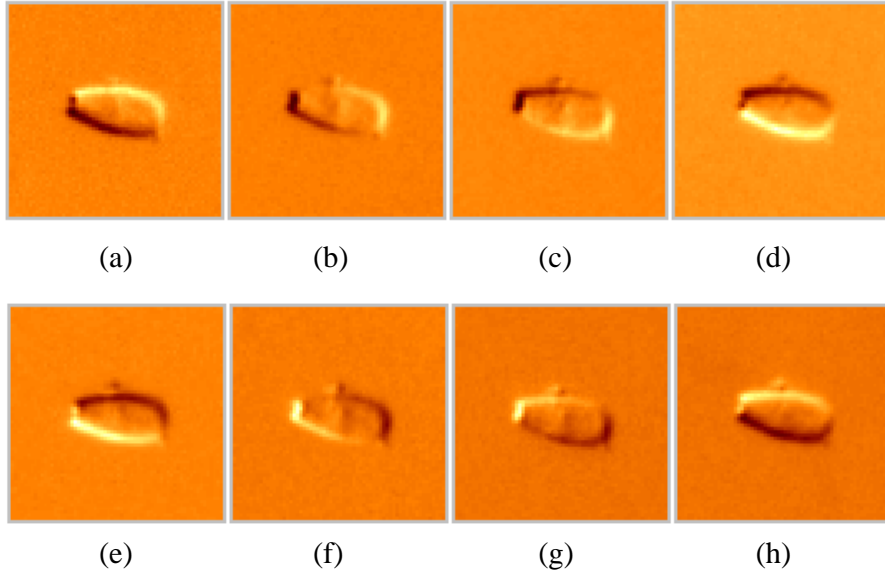


Figure 3. The images in Figure 2(b-h) were rotated so that the orientation of the shear rotates while the cell is fixed. The shear is along the 45-degrees axis in (a) and it is rotated every time approximately 45 degrees clockwise from (a) to (h).

and eight DIC images) by first subtracting the average background value from the image, and then, by setting all values less than 0.022 radians to zero. Thus, the mask has two regions: 1, a background region with pixel values equal to zero; and 2, a cell region that consists of the pixels greater than zero.

Using the same cell mask in all cases, the IOPL was computed from an estimated phase image as follows. First, an average background value of an estimated image (determined by summing the image pixels that fall within the background region of the mask) was subtracted from the estimated phase image. This is necessary because only a relative phase (or phase difference) is estimated. The phase values were converted to optical path length values

by scaling each pixel phase value with $\lambda/(2\pi)$, where λ is the wavelength of the illumination light in μm . Then the optical path-length values were summed over all pixels that fall within the cell region of the mask. Because the IOPL is computed by approximating integration with summation, the final value of the IOPL is obtained by multiplying the sum of optical path-length values by the area of the image pixel, i.e. by $(0.36\mu\text{m})^2$. Thus, the IOPL is a volume measure expressed in μm^3 .

3.4. Phase estimation with the rotational-diversity method

The corrected and aligned rotational-diversity DIC images (shown in Figure 3) were processed with the rotational-diversity method using theoretical PSFs. A PSF for the 25x/0.5-NA lens was computed using Equation 2, an empirically determined bias equal to 1.784 radians, an empirically determined shear equal to $0.72\mu\text{m}$ along the 45-degree angle, and illumination wavelength, λ , equal to 550 nm. Although the cell images were acquired with the bias set to approximately $\pi/2$ radians, the DIC bias ($2\Delta\theta$) was estimated to be equal to $1.136\pi/2$ (1.784) radians from the mean background value, I_b , of a region in the normalized DIC images with no specimen using the expression $\Delta\theta = \sin^{-1}(\sqrt{I_b})$; it is easy to show that Equation 1 reduces to $i_k(x) = \sin^2(\Delta\theta) = I_b$ for $f(x_o) = 1$. Eight rotations of the PSF were computed with a shear direction angle, γ_k , equal to 0.21, 45, 92.58, 135.77, 180.0, -46.21, -89.56, and -135.5 degrees; these angles were computed from the rotation angles estimated by the registration/alignment procedure by adding the angle of the shear direction with respect to the horizontal axis in the reference image.

For the regularization, a weight $\alpha = 2 \times 10^{-3}$ was used; this value was determined empirically by comparing images obtained at different values of α .¹² Phase images were estimated using a uniform initial guess (an image with a constant value) and different sets of rotational-diversity images, K , selected from the images shown in Figure 3: 1, from single DIC images ($K = 1$); 2, from two DIC images ($K = 2$) with shear directions at approximately 90-degrees; 3, from four ($K = 4$) and eight ($K = 8$) images with approximately 45-degree shear rotations; and 4, from four images ($K = 4$) with approximately 90 degree shear rotations. The method terminated after 70 iterations on the average.

3.5. Phase estimation with the filtering method

The corrected DIC images (shown in Figure 2) were processed with the filtering method assuming a bias of $\pi/2$ radians. The resulting phase images were then rotated according to the rotation angles determined by the registration procedure in order to compare them to the phase images obtained with the rotational-diversity method. For the Wiener filter, an empirically determined shear equal to $0.717\mu\text{m}$ along the direction that makes a 52.54-degree angle with the horizontal axis (which is equivalent to a displacement $\Delta x = 1.21$ pixels and $\Delta y = -1.58$ pixels along the x -axis and the y -axis respectively according to the procedure by van Munster *et al.*¹¹), a constant $s = 10^{12.5}$, and a constant $\sigma = 0$ were used. The values for the constants were chosen as follows. The value for s was determined empirically from a simulation study performed by van Munster *et al.*¹⁷ in which the IOPL of phantom discs with increasing area was computed with the filtering method. Because ideally the IOPL should be linear as a function of the area of the discs, the value of s that yielded the best linearity was chosen. The choice for σ is based on recent results by van Munster *et al.*¹⁷ which show that for their objectives it is better to eliminate σ , thereby, making $SN(\mathbf{u})$ (Equation 8) constant for all \mathbf{u} ; σ was initially introduced for the qualitative improvement (judged by inspection) of the appearance of the estimated images.¹¹

4. RESULTS

Results obtained with the two phase-estimation methods are presented in this section. Estimated phase images obtained from single DIC images of the same cell but at a different orientation (or equivalently with different shear direction) with the two methods are compared in Figure 4. As evident from the figure, the images computed with the rotational-diversity method are different than those computed with the filtering method. The estimated images obtained with the rotational-diversity method (Figure 4, top row) show a wide band artifact along the direction of shear. Instead of the wide band, stripes parallel to the direction of the shear are evident in the images obtained with the filtering method (Figure 4, bottom row). It was shown in a previous publication¹¹ that the severity of the stripes artifact is dependent on the value of s used for the Wiener filter in Equation 8. In fact, the choice of s is a trade-off between the band artifact and the stripes artifact.

As evident from Figure 4, a significant variability is observed in the estimated images as the shear direction changes. This variability is quantified by comparing the integrated optical path-length value (IOPL) summarized

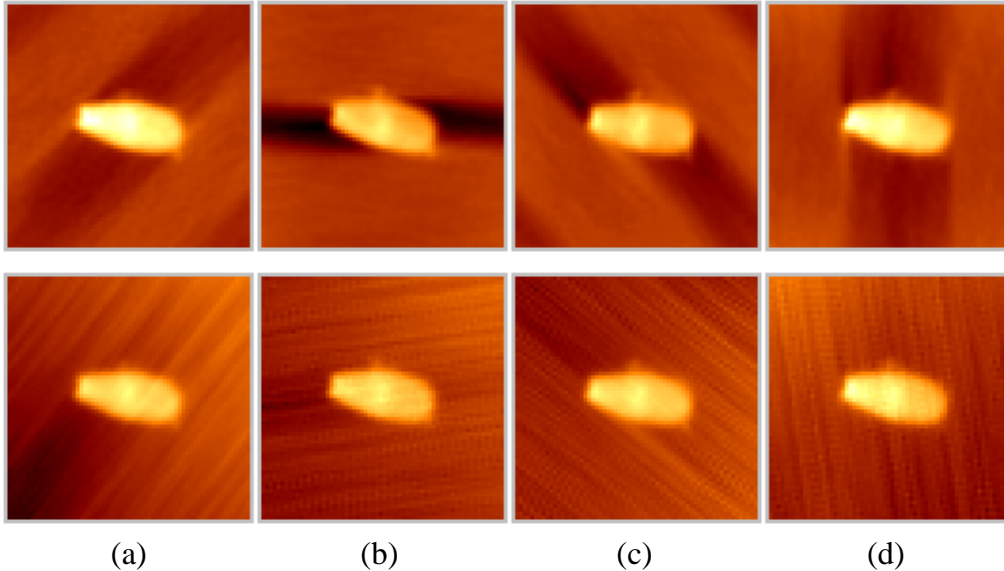


Figure 4. Estimated phase of a cell from a single DIC image with shear direction approximately along: (a) the 45-degrees axis; (b) the horizontal axis; (c) the 135-degrees axis; and (d) the vertical axis. The images were computed with the rotational-diversity method (top row) and the filtering method (bottom row).

Table 1. Effect of orientation of the cell with respect to the shear direction. γ_k is the angle the shear direction makes with the horizontal axis; IOPL_{RDM} is the IOPL computed from phase images estimated with the rotational-diversity method; IOPL_{FM} is the IOPL computed from phase images estimated with the filtering method; mean is the sample mean of the IOPL values; and st. dev. is the sample standard deviation of the IOPL values. In all cases, the IOPL was computed using the same cell mask over which the values were summed (see Section 3.3).

γ_k [degrees]	IOPL_{RDM} [μm^3]	IOPL_{FM} [μm^3]
0.2	1.220	1.341
45.0	1.789	1.410
92.6	1.653	1.599
135.8	1.546	1.264
180.0	1.222	1.262
224.5	1.819	1.414
270.4	1.618	1.486
313.8	1.325	1.456
mean	1.524	1.404
st. dev.	0.241	0.114

in Table 1 and computed as described in Section 3.3. As evident from Table 1 the IOPL values obtained with the two methods are different. The IOPL computed from the images estimated with the rotational-diversity method varies up to 20% with a maximum IOPL equal to $1.819 \mu\text{m}^3$ and a minimum equal to $1.22 \mu\text{m}^3$. For the filtering method, the variability of the IOPL is up to 14%, with maximum and minimum IOPL equal to $1.599 \mu\text{m}^3$ and $1.262 \mu\text{m}^3$ respectively. It is interesting to note that in each case, the values of the IOPL at angles, γ_k , separated by approximately 180 degrees are similar. If the variability in the IOPL value was purely due to the shear angle, then the IOPL would be expected to have a minimum at γ_k equal to 0 and 180 degrees, in which case the longest axis of the cell is parallel to the direction of shear, and a maximum at γ_k equal to 90 and 270 degrees, in which case the longest axis of the cell is perpendicular to the shear direction. However, in addition to the shear angle there are other factors that contribute to the variability of the calculated IOPL, such as: 1, differences in the DIC images

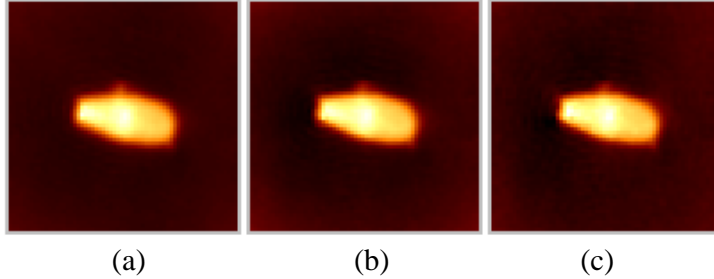


Figure 5. Estimated phase images of a cell computed with the rotational-diversity method and the images shown in Figure 3: (a) from eight images ($K = 8$); (b) from the first four ($K = 4$) images (Figure 3a-d); and (c) from two ($K = 2$) images (Figure 3b and d).

Table 2. Effect of rotational diversity on the IOPL of a cell. K is the number of rotationally-diverse images used; γ_k is the angle the shear direction makes with the horizontal axis; IOPL_{RDM} is the IOPL computed from phase images estimated with the rotational-diversity method. In all cases, the IOPL was computed using the same cell mask over which the values were summed (see Section 3.3). The sample mean and standard deviation of the IOPL_{RDM} are reported at the bottom of the table.

K	γ_k [degrees]	IOPL_{RDM} [μm^3]
2	45, -46.2	1.835
2	0.21, -89.6	1.831
4	0.21, 45, -46.2, -89.6	1.833
4	92.6, 135.8, 180, -135.5	1.854
4	45, -46.2, 135.8, -135.5	1.867
8	all of the above	1.846
mean value		1.844
stand. deviation		0.014

due to a change in the focus during specimen rotation and subsequent refocusing; and 2, error in the determination of the shear and/or rotation angle. The accuracy of the IOPL values is also affected by errors in the calculation of the IOPL such as: 1, an error in the average image background value, that needs to be subtracted from the image for the IOPL calculation, due to the band and the stripes artifacts; and 2, an error in generating the cell mask (i.e. error in deciding which pixels should be considered as part of the cell).

Results obtained with the rotational-diversity method using two or more rotationally-diverse DIC images, shown in Figure 5 and Table 2, demonstrate that the dependence of the estimated phase and IOPL values on the orientation of the cell with respect to the shear is significantly reduced. First, the images in Figure 5 do not suffer from the band or stripes artifact; this direction dependent artifact makes image segmentation for quantification more difficult and quantitative results less accurate. And second, the variability of the IOPL in Table 2 is only up to 1.3%.

5. SUMMARY AND CONCLUSIONS

In this paper, DIC images of bovine spermatozoa heads acquired by imaging the specimen at different rotation angles with respect to the shear direction were used to compare two different phase-estimation methods: 1, the filtering method¹¹; and 2, the rotational-diversity method.⁶ For the comparison, phase images were estimated from single DIC images using both methods, and from multiple (rotationally-diverse) DIC images using the rotational-diversity method. The integrated optical path length (IOPL) was computed from the phase images by summing the optical path-length values over a cell area and the variability of the IOPL was used as a performance measure.

The IOPL computed with either method from phase images of the same cell estimated from single DIC images, acquired at different orientations of the cell with respect to the shear angle, varies significantly with the shear

angle. The IOPL variability was found to be up to 20% for the rotational-diversity method and up to 14% for the filtering method. The filtering method is somewhat tuned (by the choice of a parameter as is shown in another publication¹⁷) to yield images that are less sensitive to the orientation of the cell with respect to the shear, at the expense of quantification and image quality. Phase images estimated from single DIC images (obtained with either method) were shown to suffer from artifacts that make quantification more difficult.

Such artifacts were not present in phase images computed using the rotational-diversity method and multiple DIC images. The variability in the IOPL computed from phase images estimated from two or more rotationally-diverse DIC images using the rotational-diversity method was found to be up to 1.3%. Thus, the rotational-diversity method significantly reduces the IOPL variation due to the shear angle when at least two DIC images separated by a 90-degree rotation are used for the phase estimation and has the potential to provide results that are more accurate than then filtering method.

The comparison in this paper did not address the computation time required by each phase-estimation method. As expected, the rotational-diversity method is more computationally intensive than the filtering method because it is iterative and it is based on a more complex and rigorous model than the model assumed by the filtering method. It should be noted that the rotational-diversity method is a general method that is not limited to a specific application, contrary to the filtering method which was developed for a special application in which certain model approximations may be suitable.

6. ACKNOWLEDGEMENTS

This research was supported in part by the National Institutes of Health under research grants RR 01380, BTA-SIO-RR 10412, Washington University, St. Louis, MO, and by Holland Genetics, Arnhem, the Netherlands under project No. HGKW4.

REFERENCES

1. R. D. Allen, G. B. David, and G. Nomarski. “The Zeiss-Nomarski Differential Interference Equipment for Transmitted-Light Microscopy”. *Zeitschrift für Wissenschaftliche Mikroskopie und Mikroskopische Technik*, 69(4):193–221, 1969.
2. W. Lang. “Nomarski Differential Interference Contrast Microscopy”. *A Collection of Four Articles from Zeiss Information, Carl Zeiss, 7082 Oberkochen, West Germany*, 1968.
3. C. Preza, D. L. Snyder, and J.-A. Conchello. “Imaging Models for Three-Dimensional Transmitted-Light DIC Microscopy”. In C. J. Cogswell, G. S. Kino, and T. Wilson, editors, *Proceedings of the IS&T/SPIE symposium on Electronic Imaging, Science and Technology*, volume 2655, pages 245–257, 1996.
4. T. J. Holmes and W. J. Levy. “Signal-Processing Characteristics of Differential-Interference-Contrast Microscopy”. *Applied Optics*, 26(18):3929–3939, 1987.
5. K. Dana. “Three Dimensional Reconstruction of the Tectorial Membrane: An Image Processing Method Using Nomarski Differential Interference Contrast Microscopy”. Master’s thesis, Massachusetts Institute of Technology, Massachusetts, 1992.
6. C. Preza, D. L. Snyder, and J.-A. Conchello. “Image Reconstruction for Three-Dimensional Transmitted-Light DIC Microscopy”. In C. J. Cogswell, J.-A. Conchello, and T. Wilson, editors, *Three-Dimensional Microscopy: Image Acquisition and Processing IV*, volume Proc. SPIE 2984, pages 220–231, 1997.
7. E. B. van Munster, L. J. van Vliet, and J. A. Aten. “Quantitative Interferometric Imaging Using a Conventional Differential Interference Contrast Microscope”. In A. V. Priezzhev, T. Asakura, and R. C. Leif, editors, *Optical Diagnostics of Biological Fluids and Advanced Techniques in Analytical Cytology*, volume Proc. SPIE 2982, pages 458–467, 1997.
8. C. Preza, D. L. Snyder, F. U. Rosenberger, J. Markham, and J.-A. Conchello. “Phase Estimation from Transmitted-Light DIC Images Using Rotational Diversity”. In T. Schulz, editor, *Image Reconstruction and Restoration II*, volume Proc. SPIE 3170, pages 97–107, 1997.
9. R. Barer. “Interference Microscopy and Mass Determination”. *Nature*, 169:366–367, 1952.
10. H. G. Davies and M. H. F. Wilkins. “Interference Microscopy and Mass Determination”. *Nature*, 169:541, 1952.

11. E. B. van Munster, L. J. van Vliet, and J. A. Aten. "Reconstruction of Optical Pathlength Distributions From Images Obtained by a Wide-Field Differential Interference Contrast Microscope". *Journal of Microscopy*, 188(2):149–157, 1997.
12. C. Preza. "*Phase Estimation Using Rotational Diversity for Differential Interference Contrast Microscopy*". PhD thesis, Washington University, Sever Institute of Technology, St. Louis, MO, expected May 1998.
13. J. W. Goodman. *Introduction to Fourier Optics*. McGraw-Hill Book Company, New York, 1968.
14. I. J. Good. "Non-Parametric Roughness Penalty for Probability Densities". *Nature Physical Sciences*, 224:29–30, 1971.
15. M. Aoki. *Introduction to Optimization Techniques*. The Macmillan Company, New York, 1971.
16. C. J. Cogswell, N. I. Smith, K. G. Larkin, and P. Hariharan. "Quantitative DIC Microscopy Using a Geometric Phase Shifter". In C. J. Cogswell, J.-A. Conchello, and T. Wilson, editors, *Three-Dimensional Microscopy: Image Acquisition and Processing IV*, volume Proc. SPIE 2984, pages 72–81, 1997.
17. E. B. van Munster, E. K. Winter, and J. A. Aten. "Measurement Based Evaluation of Optical Pathlength Distributions Reconstructed From Simulated Differential Interference Contrast Images". *Journal of Microscopy*, submitted, 1997.